J Physiol 589.21 (2011) pp 5125–5142

The Journal of Physiology

Kv1 channels control spike threshold dynamics and spike timing in cortical pyramidal neurones

Matthew H. Higgs[1,2] and William J. Spain[1,2,3]

[1] *Neurology Section, Department of Veterans Affairs Medical Centre, Seattle, WA, USA*
[2] *Department of Physiology & Biophysics, University of Washington, Seattle, WA, USA*
[3] *Department of Neurology, University of Washington, Seattle, WA, USA*

Non-technical summary Spiking neurones generate action potentials when the transmembrane voltage difference near the spike generating zone reaches a threshold level. Above the threshold, the inward sodium current exceeds the outward potassium current, causing the rapid upstroke of the action potential. In many neurones, including cortical pyramidal cells, the threshold is not constant but responds to a change in voltage with a short delay. The functional effect is equivalent to high-pass filtering of the voltage response, and a major benefit is enhanced spike timing precision. Two mechanisms that may contribute to a dynamic spike threshold are sodium channel inactivation and potassium channel activation, both caused by a rise in voltage. We found that blocking low-threshold Kv1 potassium channels greatly reduced threshold changes in pyramidal neurones located in layer 2–3 of the rat motor cortex. Studies using noise stimulation showed that blocking Kv1 impaired the ability of these cells to encode fast components of the input signal with precisely timed spikes. These results demonstrate a key role of Kv1 in cortical spike timing, with possible implications for information coding as well as pathological hypersynchronous discharges in epilepsy.

Abstract Previous studies showed that cortical pyramidal neurones (PNs) have a dynamic spike threshold that functions as a high-pass filter, enhancing spike timing in response to high-frequency input. While it is commonly assumed that Na^+ channel inactivation is the primary mechanism of threshold accommodation, the possible role of K^+ channel activation in fast threshold changes has not been well characterized. The present study tested the hypothesis that low-voltage activated Kv1 channels affect threshold dynamics in layer 2–3 PNs, using α-dendrotoxin (DTX) or 4-aminopyridine (4-AP) to block these conductances. We found that Kv1 blockade reduced the dynamic changes of spike threshold in response to a variety of stimuli, including stimulus-evoked synaptic input, current steps and ramps of varied duration, and noise. Analysis of the responses to noise showed that Kv1 channels increased the coherence of spike output with high-frequency components of the stimulus. A simple model demonstrates that a dynamic spike threshold can account for this effect. Our results show that the Kv1 conductance is a major mechanism that contributes to the dynamic spike threshold and precise spike timing of cortical PNs.

(Resubmitted 21 July 2011; accepted after revision 12 September 2011; first published online 12 September 2011)
Corresponding author M. H. Higgs: Veterans Affairs Puget Sound Health Care System, Neurology (Mail Stop 127), 1660 South Columbian Way, Seattle, WA 98108, USA. Email: higgsm@uw.edu

Abbreviations AIS, axon initial segment; 4-AP, 4-aminopyridine; CPP, (±)3-(2-carboxypiperazin-4-yl)-propyl-1-phosphonic acid; DNQX, 6,7-dinitroquinoxaline-2,3-dione; DTX, α-dendrotoxin; HT, high-threshold; LIF, leaky integrate-and-fire; LT, low-threshold; PN, pyramidal neurone; STA, spike-triggered average.

DOI: 10.1113/jphysiol.2011.216721

Introduction

In order to encode rapidly varying signals, neurones employ negative feedback to filter out slow components of their synaptic input. High-pass filtering facilitates precise temporal coding, compensating for variable conduction delays, slow synaptic currents, and dendritic filtering. Common high-pass mechanisms include spike frequency adaptation (Benda *et al.* 2005), time-dependent rectification of membrane currents (Hutcheon & Yarom, 2000; Hsiao *et al.* 2009), and dynamic changes of the voltage threshold for spiking (Azouz & Gray, 2000, 2003; Platkiewicz & Brette, 2011).

Changes of spike threshold were observed before the action potential was understood and were classically termed accommodation (Hill, 1936). Accommodation was seen in the squid giant axon (LeFevre, 1950), and Hodgkin & Huxley (1952) recognized that it could be explained by sodium channel inactivation and potassium channel activation. More recently, dynamic threshold changes were observed in hippocampal and cortical pyramidal neurones (PNs) *in vitro* (Stafstrom *et al.* 1984) and *in vivo* (Henze & Buzsáki, 2001; Azouz & Gray, 2000, 2003; Wilent & Contreras, 2005; Naundorf *et al.* 2006) and were explained by the same mechanisms, although without pharmacological or molecular evidence.

In addition to ion channel kinetics, the dynamics of threshold depend on the location of spike initiation in the axon initial segment (AIS) (Stuart *et al.* 1997; Palmer & Stuart, 2006; Shu *et al.* 2007; Kole & Stuart, 2008). In dual recordings from the soma and axon, Yu *et al.* (2008) found that noise injection at the soma caused less threshold variation in the proximal axon compared to the soma. These data indicate that the voltage gradient along the AIS is responsible for some of the variance of the somatic threshold, and suggest that this gradient may be an important mechanism of temporal filtering, as shown in auditory coincidence detector neurones (Kuba *et al.* 2006; Ashida *et al.* 2007). Thus, ion channels on the AIS may affect the somatic threshold by regulating the voltage gradient along the AIS before spike initiation, in addition to controlling the voltage threshold in the spike initiation zone.

In the present study, we investigated whether low-threshold Kv1 channels contribute to threshold accommodation in PNs in cortical layer 2–3. PNs here and in other cortical layers express Kv1.1 and Kv1.2 subunits on the AIS (Inda *et al.* 2006; Lorincz & Nusser, 2008; Ogawa *et al.* 2008). Consistent with this, axonal recordings have revealed large currents sensitive to the Kv1 blocker α-dendrotoxin (DTX) and the Kv1.2 selective blocker α-tityustoxin, which play a major role in repolarizing the axonal action potential (Kole *et al.* 2007; Shu *et al.* 2007). In addition, Kv1 channels have been shown to increase the spike threshold in cortical PNs (Bekkers & Delaney, 2001; Guan *et al.* 2007; Yu *et al.* 2008), but the dynamics of this effect have not been reported. Because Kv1 channels activate rapidly (Rothman & Manis, 2003; Guan *et al.* 2006; Kole *et al.* 2007; Shu *et al.* 2007), we hypothesized that they contribute to fast threshold accommodation. To test this hypothesis, we determined the effects of Kv1 blockade on the spike threshold in response to stimulus-evoked synaptic input, current steps of varied duration, and long periods of noisy current injection that simulate the natural up-states of cortical PNs. Our results indicate that Kv1 channels are a major mechanism contributing to the dynamic spike threshold of layer 2–3 PNs.

Methods

Ethical approval

All procedures complied with the National Research Council Guidelines for the Care and Use of Laboratory Animals and the principles of UK regulations, as described in Drummond (2009), and were approved by the Institutional Animal Care and Use Committee of the Seattle Veterans Affairs Health Care System.

Slice preparation and solutions

Adult (8- to 16-week-old) male Sprague–Dawley rats were deeply anaesthetized with inhaled isoflurane (4%) and killed by decapitation. A brain block containing the motor cortex was attached to a vibrating blade microtome and cut into coronal slices of 300 μm thickness. Brain blocking and slicing were performed at room temperature, either in artificial cerebrospinal fluid (ACSF) or in a sucrose-based cutting solution. No clear differences in cell viability or results were observed between the two solutions. ACSF contained the following (in mM): 125 NaCl, 3 KCl, 2 $CaCl_2$, 2 $MgCl_2$, 26 $NaHCO_3$, 1.25 NaH_2PO_4, and 20 D-glucose, bubbled with 95% O_2–5% CO_2 (carbogen). The sucrose-based cutting solution contained (in mM): 220 sucrose, 3 KCl, 1 $CaCl_2$, 5 $MgCl_2$, 26 $NaHCO_3$, 1.25 NaH_2PO_4, and 10 D-glucose, bubbled with carbogen. After cutting, slices were maintained for up to 8 h at room temperature in ACSF. For recording, a slice was transferred to a submerged chamber with a mesh support and superfused at 2 ml min^{-1} with ACSF (34°C). In all experiments using injected current stimuli, the ACSF contained 6,7-dinitroquinoxaline-2,3-dione (DNQX, 20 μM), (±) 3-(2-carboxypiperazin-4-yl)-propyl-1-phosphonic acid (CPP, 5 μM), and picrotoxin (100 μM) to block synaptic input mediated by AMPA/kainate, NMDA, and $GABA_A$ receptors, respectively. In some experiments, the recording solution contained CGP55845 (2 μM) to block $GABA_B$ receptor-mediated IPSCs, which were observed during

application of DTX or 4-AP in the presence of picrotoxin.

Recording, data acquisition, and general methods of analysis

Intracellular recordings were obtained using sharp electrodes pulled from borosilicate glass (Sutter BF100-50-10). For synaptic stimulation experiments, the electrodes were filled with 2 M potassium methylsulfate, 30 mM Mops, pH 7.2 and typically had resistances of 50–80 MΩ. For current injection studies, electrodes were filled with 3 M KCl and had resistances of 40–50 MΩ. Sharp electrode recording was chosen over the whole-cell patch electrode method because the membrane properties and firing were more stable, presumably because of the lack of intracellular wash-out and the ability to record from cells deep within the slices. In the 39 regular-spiking layer 2–3 neurones providing data for the present analyses, the input resistance was 36 ± 11 MΩ (mean ± SD) and the membrane time constant was 9.3 ± 2.4 ms. Both values were somewhat smaller than those obtained previously in patch electrode recordings from layer 2–3 PNs (55 ± 19 MΩ and 14.1 ± 3.7 ms; Higgs *et al.* 2006), which may be a consequence of membrane penetration by the sharp electrodes, less wash-out of ion channels, and/or older rats (8–16 weeks *versus* 3–5 weeks).

Current clamp recording was performed using an Axoclamp-2A amplifier (Molecular Devices, Sunnyvale, CA, USA). For synaptic stimulation experiments, recordings were obtained in bridge balance mode with 10 kHz low-pass filtering and 20 kHz data sampling. For current injection studies, in order to minimize voltage artifacts caused by electrode series resistance and capacitance, most recordings were obtained using computer-controlled discontinuous current clamp, in which current injection and voltage recording are separated in time. In each 200 μs (5 kHz) cycle, a 50 μs current injection (4 × mean current) was followed by a 150 μs relaxation period before voltage sampling. To verify that the electrode response was fast enough (with maximal capacitance compensation), each electrode was tested with current steps before cell impalement. Electrodes showing a noticeable offset at the end of the relaxation period were discarded. Data input/output was controlled by a National Instruments PCI-6221 data acquisition board connected to a Pentium PC running Real-Time eXperimental Interface software (http://www.rtxi.org) under Real-Time Application Interface Linux. Data were analysed in Igor Pro (WaveMetrics, Lake Oswego, OR, USA) and Matlab (The Mathworks, Natick, MA, USA), and spikes were detected as upward crossings of –20 mV separated by at least 2 ms.

Protocol for spike threshold accommodation in response to synaptic input

These experiments measured the spike threshold as a function of the EPSP-spike latency, or rise time from the EPSP onset to the spike. The extracellular stimuli were single pulses delivered by a constant-current stimulus isolator (World Precision Instruments) connected to a tungsten parallel bipolar electrode (FHC) positioned in layer 2–3 approximately 200–400 μm horizontal from the recorded soma. The inter-stimulus interval was 2–5 s. EPSPs having different rates of rise were evoked by varying either the stimulus duration (cycle of 0.05, 0.10, 0.15 and 0.20 ms) or the stimulus amplitude (cycle of 1, 1 $^1/_3$, 1 $^2/_3$ and 2 × threshold for evoking a postsynaptic spike in the recorded neurone). A few recordings showing apparent antidromic spikes (identified by very short latencies, very low thresholds, and no preceding EPSP) were terminated, or the stimulus polarity or position was changed to avoid direct stimulation of the axon.

The EPSP onset was measured where the voltage reached 2 mV above the mean pre-stimulus baseline, and each spike threshold ($V_{\mathrm{threshold}}$) was measured where $\mathrm{d}V/\mathrm{d}t = 40\ \mathrm{V\ s^{-1}}$ (a value high enough to distinguish spikes from EPSPs), using linear interpolation of $\mathrm{d}V/\mathrm{d}t$ *versus* V between data points. The EPSP-spike latency was taken as the time at spike threshold minus the time at EPSP onset, and the accommodation of spike threshold was measured by plotting $V_{\mathrm{threshold}}$ as a function of the latency. Over the range of latencies obtained with single-pulse EPSPs (generally 1–6 ms) these plots were approximately linear, and the strength of accommodation was measured by the slope of a line fitted to the data points by least-squares linear regression.

Threshold current step protocol

For measurement of spike threshold in response to injected current steps, each neurone was depolarized to a baseline voltage of approximately –70 mV using positive holding current, and current steps (usually 1.6, 3, 6, 12, and 24 ms) were applied at a 1 s interval. For each step duration, the step amplitude was adjusted to obtain a single spike on ∼50% of the trials by dividing the amplitude by 1.02 after each trial with a spike and multiplying by 1.02 after each trial with no spike. Because of these adjustments, the data were not suitable for investigation of spike timing jitter. However, the method was convenient for obtaining spikes with different rates of depolarization, and the maximal depolarization on trials without spikes provided a second indication of spike threshold to confirm our results.

Noise stimulation

Noise stimuli comprised a noise current (I_{noise}) and an offset (I_{offset}), which was either held constant or adjusted slowly to maintain a targeted firing rate:

$$I_{inj}(t) = I_{noise}(t) + I_{offset}(t) \quad (1)$$

I_{noise} had a standard deviation $\sigma_I = 100$ pA and a relaxation time constant $\tau_{noise} = 5$ ms and was created by a discrete-time Ornstein–Uhlenbeck process (Uhlenbeck & Ornstein, 1930) based on a Gaussian white noise term (χ) of unit standard deviation:

$$\frac{\Delta I_{noise}}{\Delta t} = \frac{-I_{noise}}{\tau_{noise}} + \frac{2\sigma_I \chi}{\tau_{noise}} \quad (2)$$

In some experiments, we maintained a fixed target firing rate (r_{target}) by adjusting I_{offset}. In order for I_{offset} to reach steady state at the target rate, I_{offset} was increased at a constant rate ($k_{offset} = 8$ pA s^{-1}) between spikes and was reduced by a small increment (ΔI_{spike}) upon detection of each spike:

$$\Delta I_{spike} = \frac{k_{offset}}{r_{target}} \quad (3)$$

In the experiments described below, r_{target} was 5 Hz. Thus, $\Delta I_{spike} = 1.6$ pA. The values of k_{offset} and ΔI_{spike} were small enough that I_{offset} was essentially direct current, and its slight variation had no apparent effect on the action potentials or the subthreshold voltage trajectories.

Spike-triggered average (STA) current

For n spikes, I_{STA} was calculated as the mean I_{noise} at a time delay τ with respect to each spike time, t_s:

$$I_{STA}(\tau) = \frac{1}{n}\sum_{s=1}^{n} I_{noise}(t - t_s) \quad (4)$$

Coherence

The strength of the phase relationship between stimulus frequency components and spikes was quantified by the coherence, which was measured using a filter bank/spike-triggered average method similar to that described by Grasse & Moxon (2010). Our filter bank was comprised of 31 cosine wavelets, $w_j(\tau)$, $j = \{0, 1, \ldots, 30\}$ with centre frequencies (f_j) evenly spaced from 1 to 1000 Hz on a logarithmic axis:

$$f_j = 10^{0.1j}\ Hz \quad (5)$$

$$w_j(\tau) = \cos(2\pi f_j \tau)\ \exp\left(\frac{-f_j^2 \tau^2}{2}\right) \quad (6)$$

In the time domain, each filter is a brief, sinusoidal waveform having a Gaussian envelope with a standard deviation equal to one cycle. In the frequency domain, the filter gain is a Gaussian function of frequency with a standard deviation of $f_j/(2\pi)$, and the phase lag is zero for all frequencies. Each stimulus frequency band, $I_j(t)$, was isolated by convolving $I_{noise}(t)$ with $w_j(\tau)$:

$$I_j(t) = I_{noise}(t) * w_j(\tau) \quad (7)$$

The coherence at each frequency was measured by sampling $I_j(t)$ over one cycle before each spike time, normalizing each $I_j(t - t_s)$ by its magnitude (determined by Fourier transformation), and computing the spike-triggered average for this frequency component of the stimulus current:

$$I_{j,STA}(\tau) = \frac{1}{n}\sum_{s=1}^{n} \frac{I_j(t - t_s)}{\left|I_j(t - t_s)\right|} \quad (8)$$

The coherence, c_j, was then estimated as the squared magnitude of $I_{j,STA}(\tau)$ and corrected for bias caused by sampling a finite number of spikes (Grasse & Moxon, 2010):

$$c_{est,j} = \left|I_{j,STA}\right|^2 \quad (9)$$

$$c_j = \frac{n c_{est,j} - 1}{n - 1} \quad (10)$$

The coherence is a dimensionless value ranging from 0 for randomly timed spikes to 1 for perfectly phase-locked spikes. The definition of coherence used here differs from the traditional definition applied to a data window of fixed width (the squared magnitude of the stimulus-response cross-spectrum divided by the magnitude of the stimulus auto-spectrum times the magnitude of the response auto-spectrum). Measuring coherence based on the STA quantifies the strength of the phase relationship between the local spike-triggering stimulus and the spikes. Using a bank of wavelet filters causes the range of time delays analysed to scale in proportion to the stimulus period ($1/f$). The rationale for this approach is that neuronal spike timing is not influenced by stimulus oscillations occurring many cycles earlier, and is therefore uncorrelated with distant stimulus oscillations unless the stimulus is exactly periodic. Thus, the local correlation is what we wish to measure.

Data and statistical comparisons

Data are expressed as means ± SEM. Statistical comparisons were performed using Student's t tests. When n pairwise comparisons were performed (e.g. control vs. drug at n time points), the results were considered

significant when $P < 0.05 / n$ (Bonferroni's correction factor).

Materials

DTX was purchased from Alomone Labs (Jerusalem, Israel), and CGP55845 was obtained from Tocris Bioscience (Ellisville, MO, USA). All other chemicals were from Sigma-Aldrich (St Louis, MO, USA).

Results

Data were obtained by intracellular recording from neurones in layer 2–3 of adult rat motor cortex slices using sharp electrodes. The data are from cells that had a resting membrane potential negative to –70 mV, fired overshooting spikes, and were regular-spiking based on their action potential waveform and ability to fire at low frequency during constant current injection. Kv1 channels were blocked using DTX (100–200 nM) or 4-AP (100 μM). DTX blocks channels containing Kv1.1, 1.2 and/or 1.6 subunits (Harvey & Robertson, 2004), whereas 4-AP potently blocks Kv1 (Castle *et al.* 1994; Russell *et al.* 1994; Stephens *et al.* 1994) and Kv3 channels (Du *et al.* 1996; Massengill *et al.* 1997). Because Kv3 channels have not been found in rodent PNs, low concentrations of 4-AP are expected to be relatively selective for Kv1 channels in these cells. The experiments described below were performed using both agents (in different cells), and similar results were obtained in all cases. Thus, all statistical comparisons were made using the pooled data from all cells tested with DTX or 4-AP.

Blocking Kv1 channels reduced threshold accommodation in response to synaptic input

As a simple protocol to investigate how Kv1 channels affect spike threshold dynamics in response to synaptic input, we applied single extracellular stimulus pulses of different strengths (see Methods) in order to vary the rate of rise of the EPSP. These experiments were performed without synaptic blockers; it was not possible to block inhibitory synaptic transmission because extracellular stimuli then triggered propagating, all-or-none epileptiform discharges. Stimuli of different strengths, generally including one just-threshold level, were applied repeatedly while the slice was superfused with control ACSF and then with ACSF containing DTX or 4-AP. It was anticipated that these agents could have presynaptic effects and change the size of the EPSP. Thus, the stimuli were adjusted during drug application in order to maintain one of the weaker stimuli at just-threshold strength, scaling all of the stimuli by the same factor. In most cases, this adjustment resulted in a similar range of spike latencies in control solution and during Kv1 blockade.

An example of the raw data is shown in Fig. 1*A*. EPSPs evoked by four stimulus strengths are shown by blue, green, orange and red traces (each truncated at the first action potential). Each spike threshold ($V_{\mathrm{threshold}}$) (measured at $\mathrm{d}V/\mathrm{d}t = 40\ \mathrm{V\ s^{-1}}$) is indicated by a dot of corresponding colour. The EPSPs evoked by the weakest stimulus reached threshold on a subset of trials, whereas the EPSPs evoked by stronger stimuli all reached threshold. For the just-threshold stimulus, spikes occurred before the peak of the subthreshold EPSPs, particularly in control ACSF (left panel). This observation is consistent with threshold accommodation, because the flat voltage trajectory at the peak of the EPSP will not intercept a rising threshold.

To illustrate the variation of threshold, we constructed phase plots (Fig. 1*B*) showing $\mathrm{d}V/\mathrm{d}t$ *versus* V at the onset of each spike. The threshold is the voltage where $\mathrm{d}V/\mathrm{d}t$ begins to increase rapidly. In control ACSF (left panel), it is apparent that the threshold was higher for the weakest stimulus (blue traces) than for the stronger stimuli, whereas in the presence of DTX (right panel) the difference appears to be less. To measure this effect, each $V_{\mathrm{threshold}}$ was plotted as a function of the EPSP-spike latency (the time from the EPSP onset to the spike threshold) (Fig. 1*C*). Over the range of latencies obtained, these curves were nearly linear. Thus, the strength of accommodation was measured by the slope of a linear fit. For each neurone ($n = 4$ with DTX, $n = 7$ with 4-AP), we compared the slope of the threshold–latency relationship in the presence of drug to the slope in control ACSF (Fig. 1*D*). For the pooled data, the mean slopes were $1.15 \pm 0.15\ \mathrm{mV\ ms^{-1}}$ in control ACSF and $0.37 \pm 0.06\ \mathrm{mV\ ms^{-1}}$ in the presence of DTX or 4-AP ($P = 0.0006$). This change in threshold accommodation was associated with only minor changes in baseline membrane potential (control, -73.5 ± 1.6 mV; DTX/4-AP, -75.1 ± 1.6 mV) and action potential width, measured at 50% height from the threshold to the peak (control, 0.51 ± 0.01 ms; DTX/4-AP, 0.56 ± 0.01 ms). Based on previous studies (Guan *et al.* 2007) and our other experiments using current injection (described below) DTX and 4-AP had little effect on the input resistance of layer 2–3 PNs, and generally caused very little change in the voltage response until just before spike threshold. Thus, the major functional effect of Kv1 that was visible at the somatic recording site was a change in the level and dynamics of spike threshold.

These data show that Kv1 plays a major role in fast threshold accommodation. However, changes in other conductances may also contribute to threshold variation. In particular, fast sodium channel inactivation is widely believed to be responsible for threshold dynamics. While the present studies were focused on the effects of Kv1,

we also measured the maximal rate of rise of each action potential as an indicator of sodium channel availability. We observed only a small decrease in rate of rise as a function of the stimulus strength and the resulting EPSP-spike latency (Fig. 1*E*). Based on linear fitting, the rate of rise decreased by 1.4 ± 0.4% per millisecond of latency in control ACSF and fell by 0.8 ± 0.5% per millisecond in the presence of DTX or 4-AP (not significantly different from control). These data provide little indication that sodium channel inactivation contributed to threshold accommodation or to the effect of Kv1 blockade. However, it remains possible that the axonal sodium channels involved in spike initiation inactivated to a greater degree than the somatic channels; investigation of this hypothesis would require different experimental methods.

Blocking Kv1 reduced threshold accommodation in response to injected current steps

The experiments described provided strong evidence that Kv1 channels contribute to threshold accommodation in response to physiological input, but had some limitations. The relatively brief, single-shock EPSPs depolarized the

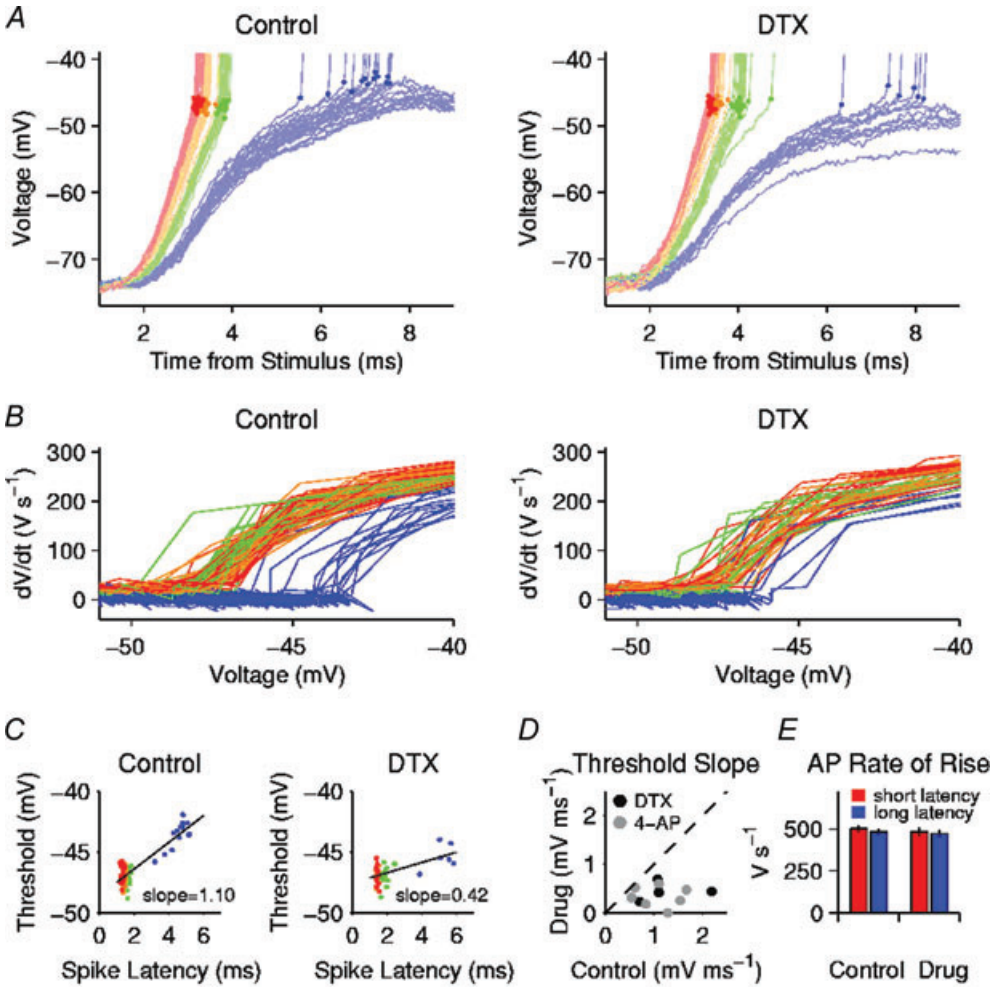

Figure 1. Kv1 blockade reduced threshold variation as a function of EPSP-spike latency
A, EPSPs evoked by stimuli of increasing strength (blue, green, orange and red). Dots mark the spike thresholds. Left panel is data obtained in control ACSF; right panel is data from the same neurone in the presence of DTX. *B*, phase plots showing d*V*/d*t versus V* for the same trials. In control solution (left) the threshold voltage (where d*V*/d*t* increased rapidly) was clearly higher for the weak stimuli (blue) than for stronger stimuli. In the presence of DTX (right) this difference was less. *C*, left, spike threshold *versus* latency (time from EPSP onset to threshold) for the same cell in control ACSF. Continuous line is a linear fit. Right, spike threshold *versus* latency in the presence of DTX. *D*, scatter plot summarizing the data from multiple neurones, comparing the slope of each cell's threshold-latency curve in the presence of drug (vertical axis) to the slope in control ACSF (horizontal axis). Black symbols indicate DTX data ($n = 4$); grey symbols indicate 4-AP ($n = 7$). *E*, average maximal rate of rise of each action potential (AP) in control ACSF and in the presence of drug (DTX or 4-AP, total $n = 11$). 'Short latency' (red) indicates the strongest stimulus for each cell. 'Long latency' (blue) indicates the just-threshold stimulus.

neurones into the range where Kv1 channels activate (above approximately –70 mV) for only short periods before reaching threshold, and the threshold did not reach a maximum when plotted as a function of the spike latency. Another concern was that DTX or 4-AP might affect the threshold indirectly by changing the synaptic input to the recorded neurone. In particular, synaptic inhibition to the axon initial segment might influence the threshold. To address these issues, our other experiments were performed using intracellular current stimuli in slices superfused with synaptic blockers (see Methods).

In these studies, the baseline membrane potential of each neurone was depolarized to approximately –70 mV with positive holding current, and just-threshold current steps of different lengths (1.6, 3, 6, 12, and 24 ms) were injected repeatedly in control ACSF and during application of DTX ($n = 6$) or 4-AP ($n = 7$). The amplitude of each current step was adjusted trial-by-trial by computer in order to maintain a just-threshold level. Thus, each step elicited either one spike (generally near the end of the step) or no spike. Typical responses are illustrated in Fig. 2*A* (control) and 2*B* (DTX), showing superimposed responses from multiple trials (grey lines). The mean responses on trials without a spike are indicated by black lines, showing the maximal depolarizations obtained without reaching threshold. In control ACSF the maximal subthreshold voltage increased as a function of step length, consistent with threshold accommodation; in the presence of DTX this increase was largely eliminated.

For each spike, $V_{threshold}$ was measured where $dV/dt = 20\ V\ s^{-1}$, a level high enough to distinguish spikes from subthreshold voltage changes in all of our current injection studies. The mean $V_{threshold}$ increased as a function of step length in control ACSF but showed less change in the presence of DTX ($n = 6$, Fig. 2*C*) or 4-AP ($n = 4$, Fig. 2*D*). Based on the pooled data for both drugs, Kv1 blockade significantly lowered $V_{threshold}$ ($P < 0.01$ for 5 paired comparisons) for 6, 12, and 24 ms steps. The

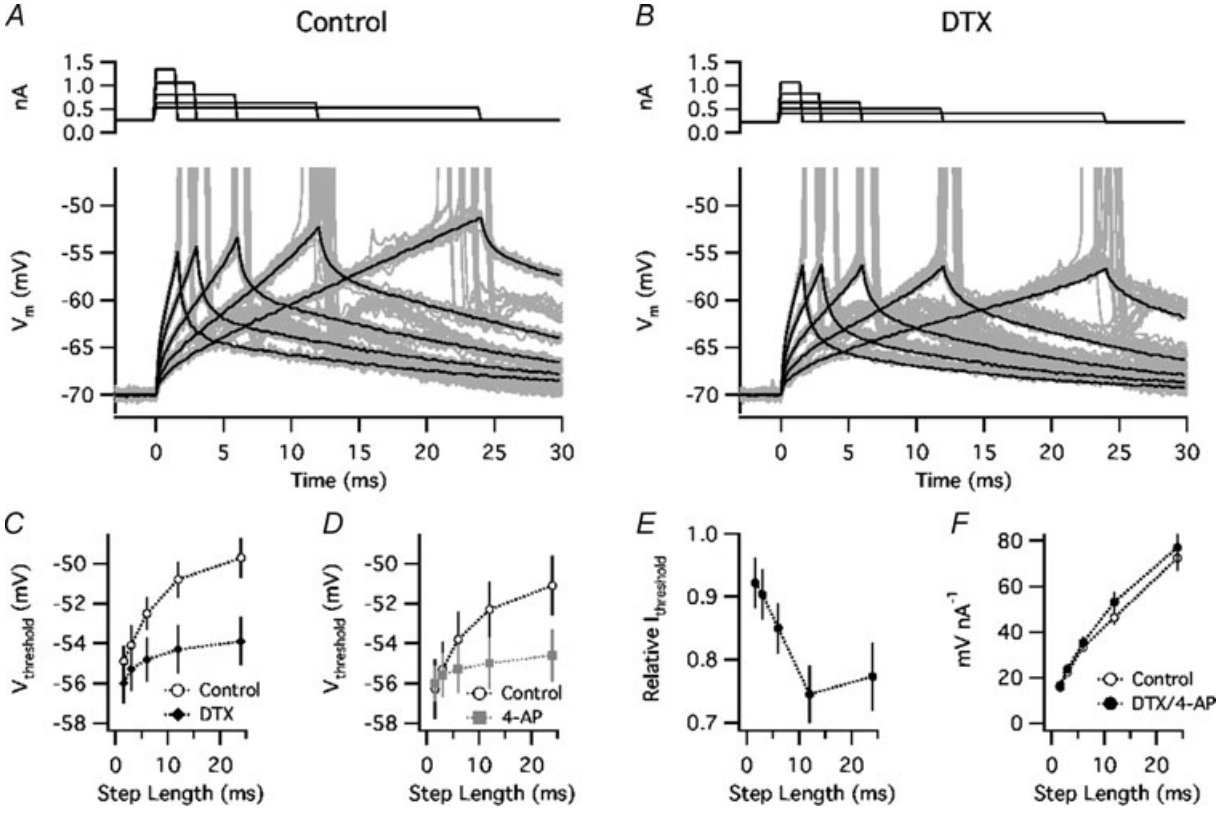

Figure 2. Kv1 blockade reduced the threshold for long but not short current steps
A, responses to current steps of peri-threshold amplitude in control ACSF. Top, mean current steps. Bottom, voltage responses on each trial (grey) and mean response on trials with no spike (black). It is apparent that larger depolarizations remained below threshold during longer steps, showing an increase in the functional voltage threshold. *B*, responses to peri-threshold current steps during application of DTX, showing little change of the maximal subthreshold depolarization as a function of step length. *C*, mean $V_{threshold}$ ($n = 6$) in control solution (open symbols) and in the presence of DTX (filled symbols), plotted as a function of step length. *D*, mean $V_{threshold}$ ($n = 4$) in control solution (open circles) and in the presence of 4-AP (filled grey symbols). *E*, relative current threshold ($I_{threshold}$) (value in drug/value in control ACSF; pooled data for DTX and 4-AP). *F*, subthreshold response amplitude, normalized by injected current.

pooled data also showed a tendency for Kv1 blockade to reduce current threshold ($I_{threshold}$) for the longer steps (Fig. 2*E*) ($P = 0.02$ for 12 ms, $P = 0.04$ for 24 ms). DTX and 4-AP did not significantly affect the amplitude of the subthreshold response to current steps of any length (Fig. 2*F*), suggesting that the Kv1 conductance had little effect on the input resistance at the soma, as reported previously (Guan *et al.* 2007).

The results of these current injection studies confirm that Kv1 channels play a major role in fast threshold accommodation, independent of any presynaptic effects. Kv1 blockade had little effect on $V_{threshold}$ for the shortest current steps, suggesting that the Kv1 conductance was not substantially activated at the baseline voltage (approximately –70 mV). However, Kv1 began to increase $V_{threshold}$ within several milliseconds of depolarization. While our experiments did not directly measure the kinetics of the threshold change with respect to $V(t)$ (because current steps do not cause step changes in voltage), the data are generally consistent with the fast activation kinetics of the axonal Kv1 current (Kole *et al.* 2007; Shu *et al.* 2007).

Threshold accommodation in response to current ramps

A limitation of the current step method was that pre-spike accommodation over longer periods could not be investigated, because the maximal time to the first spike during a long, square current step did not consistently exceed a few tens of milliseconds. To determine whether additional accommodation occurs over longer times, five neurones were injected with a set of 10 ramp currents having slopes ranging from 0.001 nA ms^{-1} to 1 nA ms^{-1} (Fig. 3). Each ramp began at zero current; no holding current was used in this set of experiments. To prevent excessive stimulation and avoid the need for a long recovery interval between trials, each ramp was terminated on detection of the first spike. Ramps were delivered at a 2 s interval in control ACSF (with synaptic blockers) and during application of 4-AP. $V_{threshold}$ was measured at 40 V s^{-1}, which was sufficient to distinguish each spike onset from the fastest pre-spike depolarizations at high ramp slopes. In control solution, $V_{threshold}$ fell by an average of ~4 mV as the ramp slope was increased from approximately 0.01 nA ms^{-1} to 0.2 nA ms^{-1} but showed little change outside this range (Fig. 3*B*). In the presence of 4-AP, $V_{threshold}$ was largely insensitive to the ramp slope. To compare these data to the step data, we plotted $V_{threshold}$ as a function of the time over which V_m rose from –70 mV (the baseline potential for step experiments) to threshold (Fig. 3*C*). The data show that the 4-AP sensitive accommodation increased as the time above –70 mV was lengthened up to approximately 25 ms, but $V_{threshold}$ remained nearly constant during longer, slower depolarizations.

Blocking Kv1 channels reduced threshold variation during noise stimulation

The studies described above were limited to relatively brief stimuli. We next investigated whether Kv1 channels contribute to threshold dynamics during longer-duration, noisy current injections that simulate the prolonged barrages of synaptic input and irregular firing observed *in vivo*. These current stimuli were comprised of Gaussian noise added to a depolarizing offset (I_{offset}). In order to focus on threshold changes caused by the subthreshold voltage trajectory rather than relative refractoriness accumulating after spikes, most experiments utilized a slow, automated adjustment of I_{offset} to hold the mean firing rate at 5 Hz (see Methods). On average, I_{offset} was lowered from 539 ± 67 pA in control ACSF to 475 ± 61 pA in the presence of DTX ($n = 4$) or 4-AP ($n = 9$).

A complication encountered in these experiments was that some neurones showed abnormal bursting in the presence of DTX or 4-AP. Most of these cells fired two-spike bursts with abnormally long intra-burst intervals of 10–20 ms, as compared to a typical intra-burst interval of ~4 ms (Higgs & Spain, 2009), and the second spike in each burst arose from an unusually low, variable threshold. These observations suggested that the second spike initiated at an ectopic site, likely to have been due to axonal hyperexcitability (Zhou *et al.* 1999; Dodson *et al.* 2003). Because this bursting appears to be pathological and was not a prerequisite for any of our other observations, data showing this effect were excluded from the following analysis. We note that our experiments using synaptic stimuli described above were not subject to this complication, because the presumed ectopic spikes were seldom observed in the absence of synaptic blockers.

The threshold variation seen during noise stimulation is illustrated in Fig. 4*A* and *B*. A phase plot of dV/dt *versus* V (Fig. 4*C*) shows that DTX had only slight effects on the somatic action potential waveform, as reported by Shu *et al.* (2007) and Kole *et al.* (2007), while the rapidly rising portion of the phase plot (Fig. 4*D*) shows that DTX lowered the threshold and reduced its variation. Kv1 blockade lowered the mean $V_{threshold}$ from –52.6 ± 0.9 mV to –56.6 ± 0.9 mV ($P = 0.005$) (Fig. 4*E*) and reduced the SD of $V_{threshold}$ from 1.02 ± 0.06 mV to 0.57 ± 0.06 mV ($P = 0.00002$) (Fig. 4*F*). Similarly, in four neurones tested without adjusting I_{offset}, 4-AP reduced the SD of $V_{threshold}$ from 0.93 ± 0.05 mV to 0.57 ± 0.04 mV in 4-AP ($P = 0.01$). These data indicate that Kv1 channels are responsible for a large portion of the threshold variation in response to a prolonged, noisy stimulus that simulates *in vivo* synaptic input.

Kv1-dependent threshold dynamics provided selectivity for fast-rising input

Our data and previous studies (Azouz & Gray, 2000, 2003) showed that the spike threshold varies as a function of the pre-spike voltage trajectory, which depends on the time course of synaptic or injected current. To investigate how threshold variations observed during noise stimulation were correlated with the stimulus waveform, we measured the spike-triggered average current (I_{STA}). The analysis was performed for the data obtained at constant mean firing rate, allowing us to distinguish specific effects on stimulus selectivity from more general effects of changing the overall firing probability. I_{STA} was computed based on I_{noise}, excluding I_{offset}. Thus, its expected value approaches zero at a long time delay under all conditions.

A typical effect of DTX on I_{STA} is illustrated in Fig. 5*A*. Although DTX had relatively little effect on the overall waveform of I_{STA} (top), it greatly reduced the slope (dI_{STA}/dt, bottom) shortly before spike onset. On average, DTX ($n = 4$) or 4-AP ($n = 9$) had a small, non-significant effect on the peak amplitude of I_{STA} (92 ± 1% of control, $P = 0.10$, Fig. 5*B*) but greatly reduced the maximal slope, which was measured with a 1 ms sliding window (48 ± 3% of control, $P = 0.000001$, Fig. 5*C*).

It is important to note that the waveform of I_{STA} depends on the correlation time scale of the stimulus (in this case, $\tau_{noise} = 5$ ms) as well as the properties of the neurone. Because of causality, only points to the left of zero time delay depend on the cell properties, whereas after zero delay I_{STA} decays exponentially with a time constant equal to τ_{noise}. If the neurone were simply a detector of current

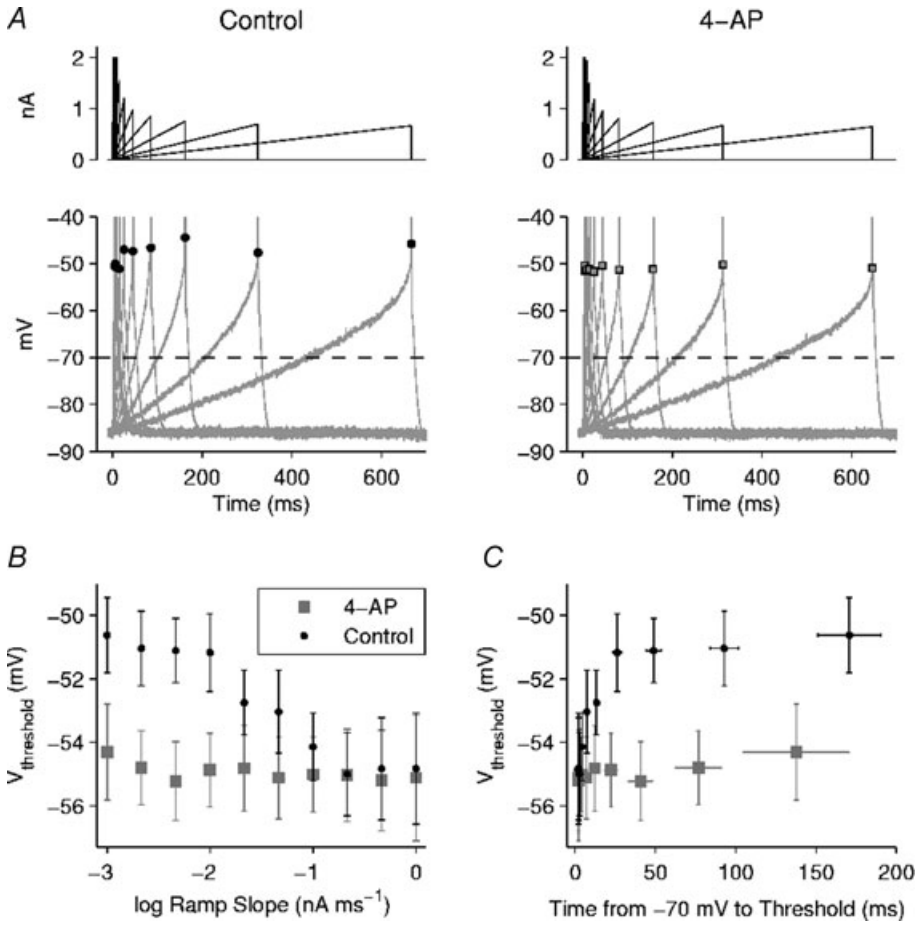

Figure 3. Kv1-dependent threshold accommodation in response to ramp currents
A, left, example of ramp currents (top) and the resulting voltage responses (bottom) in control ACSF. Each ramp was terminated on detection of the first spike (truncated on plot). Each $V_{threshold}$ is indicated by a black dot. Right, responses of the same neurone in the presence of 4-AP. Each $V_{threshold}$ is indicated by a grey-filled square. *B*, mean $V_{threshold}$ *versus* ramp slope (in log units) ($n = 5$ cells). In control ACSF (black dots) $V_{threshold}$ fell as the ramp slope was increased from approximately 0.01 nA ms^{-1} to 0.2 nA ms^{-1} but was relatively insensitive to changes outside this range. In the presence of 4-AP (grey squares), $V_{threshold}$ was nearly constant across all ramp slopes tested. *C*, mean $V_{threshold}$ *versus* time over which V_m rose from –70 mV to threshold (plotted for comparison with step current studies starting from –70 mV). In control solution, $V_{threshold}$ increased for depolarization times up to approximately 25 ms but showed little further change with slower depolarizations.

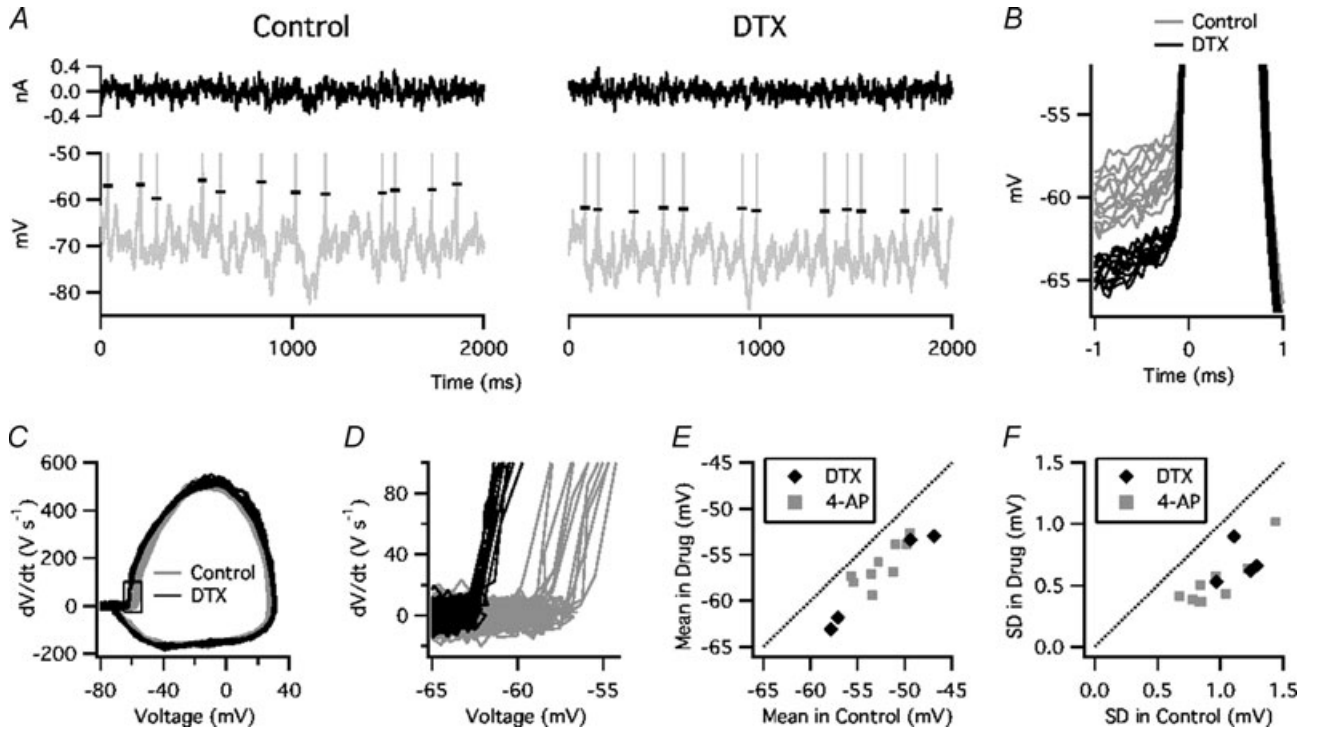

Figure 4. Kv1 blockade reduced threshold variation during noise stimulation
A, noise current (top) and voltage response (bottom, spikes truncated) in control ACSF (left) and in the presence of DTX (right). Horizontal marks indicate $V_{threshold}$. *B*, expanded view of spike onsets in control solution (grey) and during application of DTX (black). *C*, phase plot of d*V*/d*t versus V* in control solution and in the presence of DTX. *D*, expanded view of boxed region in *C*. *E*, mean $V_{threshold}$ of each cell in DTX or 4-AP (vertical axis) *versus* control (horizontal axis). *F*, SD of $V_{threshold}$ in DTX or 4-AP *versus* control.

amplitude, I_{STA} would have the same time constant on the left and right sides, reflecting the autocorrelation of the stimulus. In a cell that functions as an integrator, in which the spike response depends on the accumulated current input over some interval, the rising phase of I_{STA} would be slower than τ_{noise}. In contrast, in a differentiator neurone where the spike response depends on the rate of change of the current input, the rising phase of I_{STA} would be faster than τ_{noise}. Our control data showed that layer 2–3 PNs have an integrator-like property on a long time scale (a slow rise of I_{STA} until approximately 2 ms before the spike time) and a differentiator property on a short time scale (a fast rise of I_{STA} for 1–2 ms before the peak). During Kv1 blockade the integrator function appeared largely unaltered, whereas the differentiator function was not evident. Previous studies found similar effects of Kv1

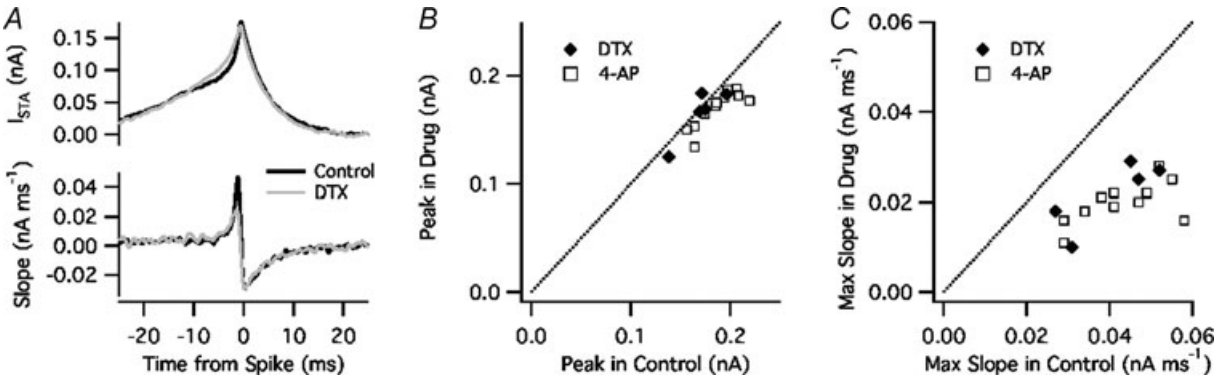

Figure 5. Kv1 blockade reduced the selectivity for fast-rising current
A, top, spike-triggered average current (I_{STA}) in control ACSF (black) and DTX (grey). Bottom, slope of I_{STA}, calculated with a 1 ms sliding window. *B*, peak amplitude of I_{STA} in DTX or 4-AP (vertical axis) *versus* control (horizontal axis). *C*, maximal slope of I_{STA} in DTX or 4-AP *versus* control.

blockade on I_{STA} in auditory brainstem neurones (Svirskis *et al.* 2002; Slee *et al.* 2005).

To investigate whether the selectivity for fast-rising current was associated with the variation of spike threshold, we computed I_{STA} and its slope separately for low-threshold (LT) spikes and high-threshold (HT) spikes. LT spikes were defined as those with $V_{threshold}$ below the mean (calculated in 10 s time bins), and HT spikes were those with $V_{threshold}$ above the mean. The analysis was performed for data obtained in control ACSF (Fig. 6*A*) and during Kv1 blockade (Fig. 6*B*). In the example shown, I_{STA} had a greater amplitude and maximal slope for LT *versus* HT spikes in control solution but showed little dependence on the spike threshold in the presence of 4-AP. These data suggest that the small variation of $V_{threshold}$ that remained during Kv1 blockade was random, probably representing the random error of our voltage data. While this example was an extreme case, significant effects in this direction were observed in our pooled data ($n = 4$ in DTX, $n = 9$ in 4-AP). In control ACSF, the maximal slope of I_{STA} was 51 ± 4 pA ms^{-1} for LT spikes *versus* 36 pA ms^{-1} for HT spikes ($P = 0.002$) (Fig 6*C*). However, in the presence of DTX or 4-AP, the maximal slope did not differ significantly between LT and HT spikes (25 ± 1 pA ms^{-1} and 21 ± 2 pA ms^{-1}, respectively) (Fig. 6*D*). These data indicate that changes in threshold caused by Kv1 channels make layer 2–3 PNs more selective for fast-rising input.

Kv1 channels increased the coherence of spike output with high-frequency input

To further characterize how Kv1 affected the response to each component of the noise stimulus, we measured the coherence of the spike output with multiple frequency bands present in the noise. The analysis was performed using a bank of wavelet filters centred at frequencies from 1 to 1000 Hz (see Methods) and was similar to the filter bank method of coherence estimation described by Grasse & Moxon (2010). The coherence quantifies the strength of phase-locking between the spike output and each frequency component of the stimulus, having a value ranging from 0 when spikes occur at random phases to 1 when all spikes occur at the same phase.

We first measured the effects of 4-AP ($n = 5$) on the coherence for noise stimuli added to a fixed I_{offset} (Fig. 7*A*). The control data showed highest coherence near 10 Hz, a nearly flat shoulder from approximately 50 to 300 Hz, and a rapid decline at higher frequencies. 4-AP slightly increased the frequency of maximal coherence and greatly reduced the coherence above 60 Hz. In experiments where

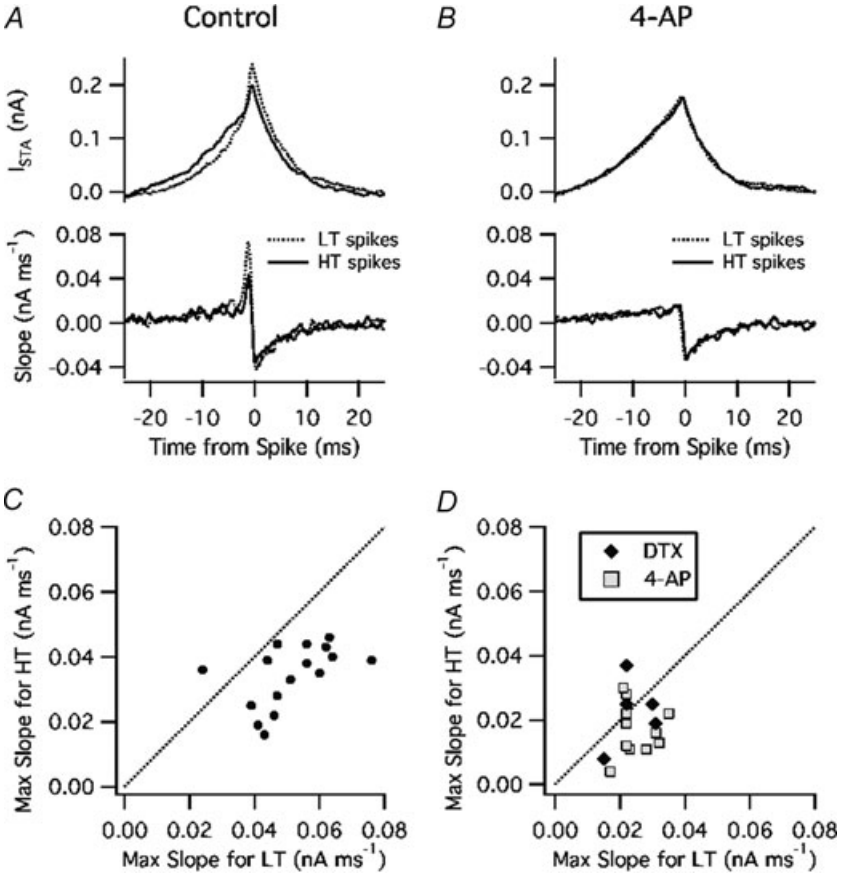

Figure 6. Kv1 blockade reduced the association between d*I*/d*t* and spike threshold
A, I_{STA} (top) and its slope (bottom) in control ACSF for low-threshold (LT) spikes (dashed line) and high-threshold (HT) spikes (continuous line). *B*, same analysis for data obtained in the presence of 4-AP. *C*, control data: maximal slope of I_{STA} for HT spikes (vertical axis) *versus* LT spikes (horizontal axis). *D*, DTX and 4-AP data: same analysis.

I_{offset} was adjusted to maintain a firing rate of 5 Hz ($n = 4$ in DTX, $n = 9$ in 4-AP), drug application caused little change in the low-frequency peak but reduced coherence at high frequencies (Fig. 7*B*). The absolute difference in coherence attributed to Kv1 was largest at ~250 Hz (Fig. 7*C*). These data suggest that Kv1 channels affect spike coherence with low-frequency input by controlling the firing rate, and increase coherence with high-frequency input by influencing the precise timing of each spike, largely independent of any change in the overall firing rate.

As an additional test of how Kv1 channels affect spike timing by a high-frequency signal, we added a sine wave current (300 Hz, 100 pA) to the noise stimulus. The mean firing rate was held at ~5 Hz as described above. The sine wave phase at which each spike occurred was determined, and a phase histogram was constructed (Fig. 7*D*). Application of 4-AP increased the width of the phase histogram, as quantified by the SD of a Gaussian fit ($n = 6$, $P = 0.0004$, Fig. 7*E*). These data confirm that Kv1 channels improve spike timing with respect to high-frequency input. The basis of this effect may be understood by considering a simple model of the dynamic spike threshold.

A simple model of the dynamic threshold

Because some aspects of our analysis (e.g. coherence) were somewhat abstract, it may be useful to consider how high-pass filtering can arise from the general function of a dynamic threshold, independent of the specific biophysical implementation. For this purpose, we constructed a simple, non-biophysical model – a leaky integrate-and-fire

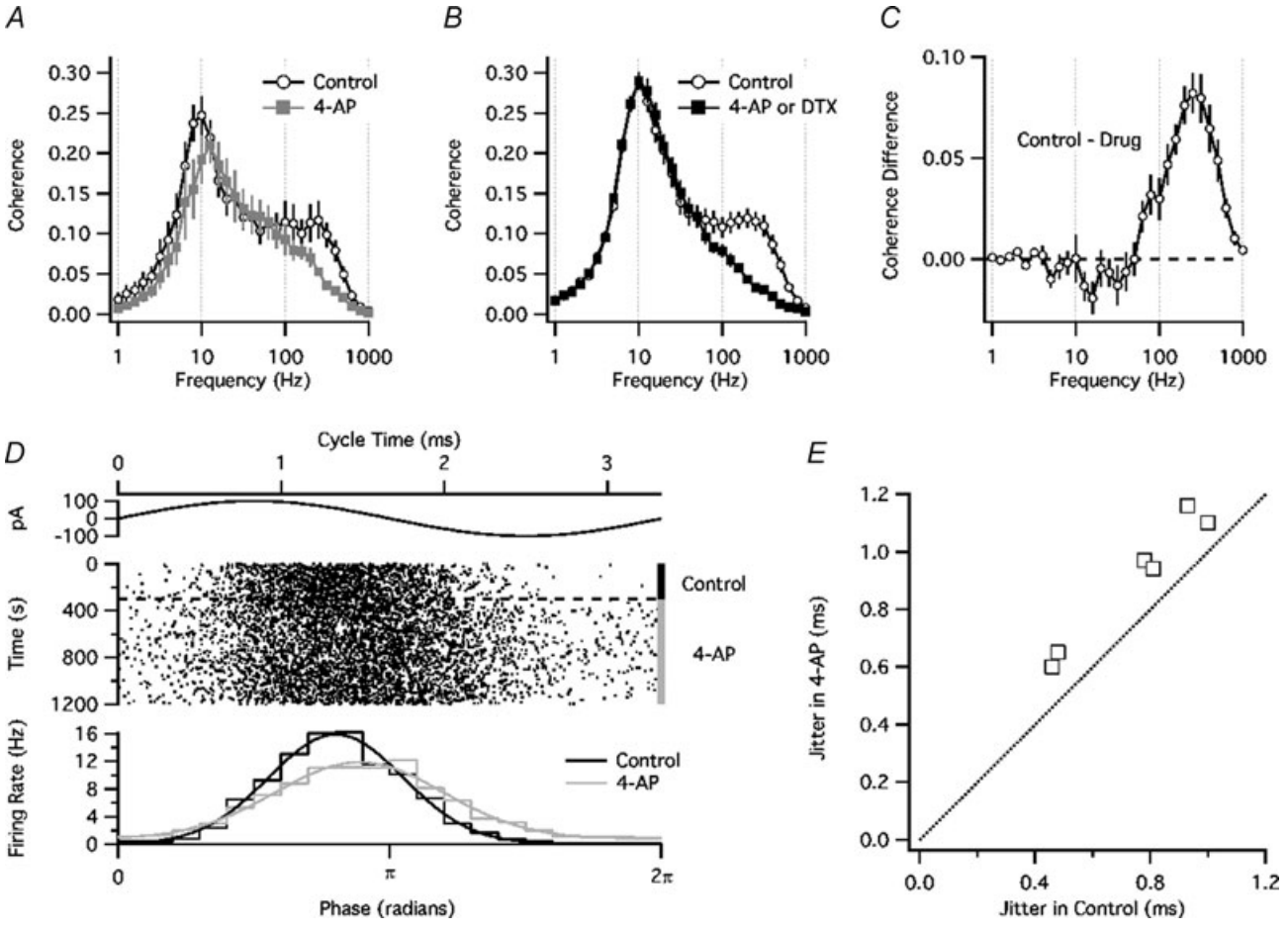

Figure 7. Kv1 blockade reduced spike coherence with high-frequency input
A, coherence *versus* frequency for experiments without firing rate control ($n = 5$). *B*, coherence *versus* frequency for experiments in which the mean firing rate was held at ~5 Hz by adjusting I_{offset} ($n = 4$ with DTX, $n = 9$ with 4-AP). *C*, difference in coherence between control ACSF and DTX or 4-AP (same experiments as in *B*). *D*, effect of 4-AP on spike timing with respect to a high-frequency sine wave current (300 Hz, 100 pA) added to noise. Top, sine wave current. Middle, spike raster. Bottom, spike phase histograms for control ACSF (black) and 4-AP (grey) with Gaussian fits. *E*, spike jitter (SD of Gaussian fit) in the presence of 4-AP (vertical axis) *versus* control (horizontal axis).

(LIF) neurone with dynamic threshold – in which the threshold was treated as a dynamical variable, $\theta(t)$. A similar approach was employed by Farries *et al.* (2010) to model the dynamic spike threshold of neurones in the subthalamic nucleus. Because our knowledge of the ion channel distribution and properties of layer 2–3 PNs is far from complete, we do not attempt to relate $\theta(t)$ to the underlying biophysics, but instead consider a simplified description of the threshold dynamics with parameters chosen based on our experimental data.

The steady-state threshold (θ_{ss}, Fig. 8*A*) was modelled as an exponential function of V:

$$\theta_{ss}(V) = \theta_{min} + (\theta_{base} - \theta_{min}) \exp\left(\frac{V - \theta_{base}}{K}\right)$$

where θ_{min} is the mimimum threshold, θ_{base} is the rheobase threshold (where a slowly changing V reaches θ), and K is the 'slope factor' or sharpness of $\theta_{ss}(V)$. A rheobase exists (and thus the neurone can fire in response to slow depolarization) if $\theta_{base} - \theta_{min} \leq K$. The dynamics of θ were simulated as a first-order relaxation with a time constant τ_θ:

$$\frac{d\theta}{dt} = \frac{\theta_{ss} - \theta}{\tau_\theta}$$

The model parameters chosen were $\theta_{min} = -55$ mV, $\theta_{base} = -50$ mV (control) or –55 mV ('DTX'), $K = 5$ mV, and $\tau_\theta = 1$ ms. The rationale for these parameters was as follows. $\theta_{min} = V_{threshold}$ for short current steps. $\theta_{base} = V_{threshold}$ for long steps. $K \geq \theta_{base} - \theta_{min}$ in order for a rheobase to exist, but must approach the minimum value (5 mV) in order to account for the strong coherence at high frequencies (see below). After fixing these parameters, τ_θ was chosen to reproduce the time course of threshold accommodation.

The dynamic threshold was added to an LIF model neurone with a resting potential and post-spike reset of –70 mV, a membrane resistance of 50 MΩ, and a

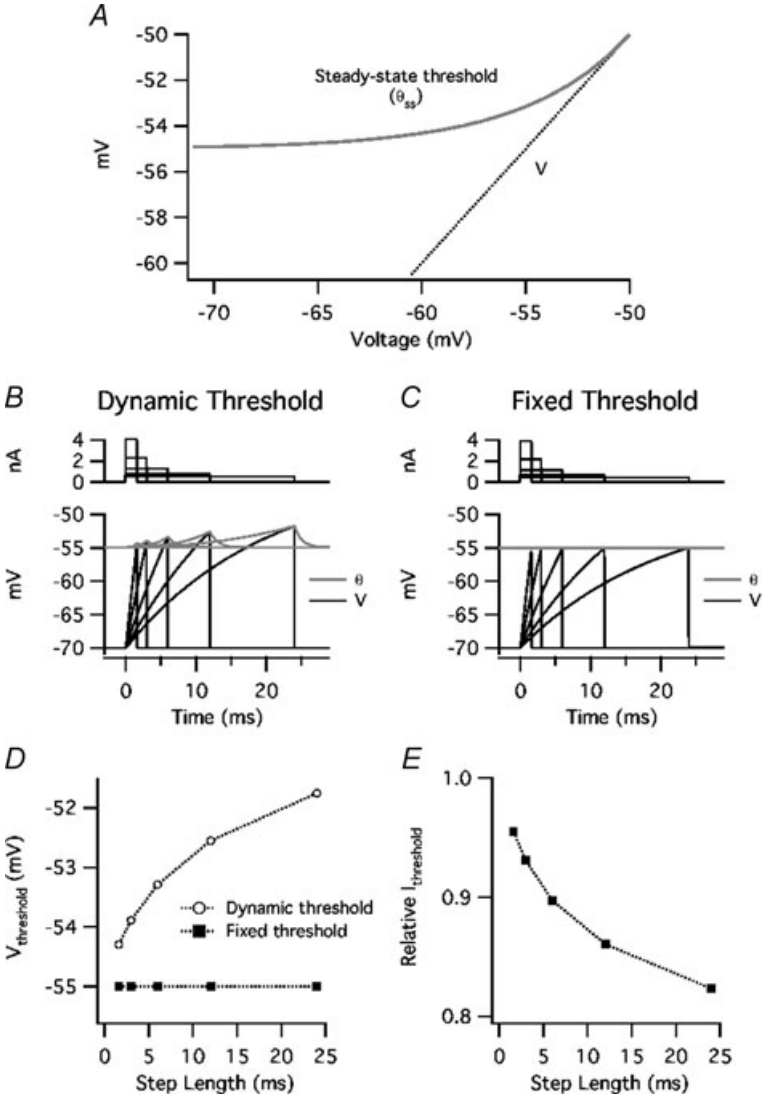

Figure 8. Dynamic threshold model: response to threshold current steps
A, steady-state threshold of model (θ_{ss}) as a function of voltage (V). The point where θ_{ss} converges with V is the rheobase threshold (θ_{base}). *B*, response to just-threshold current steps in leaky integrate-and-fire (LIF) model neurone with dynamic threshold. Top, current. Bottom, $V(t)$ (black) and dynamic threshold, $\theta(t)$ (grey). The model generates a spike and resets V at the end of each step, where $V(t)$ reaches $\theta(t)$. *C*, response to just-threshold current steps in LIF model with fixed threshold. *D*, threshold-crossing voltage ($V_{threshold}$) as a function of step length in model with dynamic threshold (open symbols) or fixed threshold (filled symbols). *E*, relative current threshold ($I_{threshold}$) (value in fixed-threshold model/value in dynamic-threshold model).

capacitance of 400 pF. The responses to just-threshold current steps (1.6, 3, 6, 12, and 24 ms) are shown in Fig. 8*B* (control) and 8*C* (fixed θ). The threshold-crossing voltage ($V_{\text{threshold}}$) increased as a function of step length (Fig. 8*D*), as observed in PNs (Fig. 1). The apparent time constant of this curve is similar to our experimental data, and is much longer than τ_θ because of the time course of $V(t)$ and the non-linearity of $\theta_{ss}(V)$. The 'DTX' condition (θ fixed at $\theta_{\min}$) lowered the current threshold, having a greater relative effect for long steps (Fig. 8*E*).

The model was also tested with the noise current used in our experiments, adjusting the DC offset to maintain a mean firing rate of 5 Hz. $\theta(t)$ varied in response to the inter-spike voltage trajectories (Fig. 9*A*), resulting in a $V_{\text{threshold}}$ that varied among spikes (Fig. 9*B*). Fixing θ lowered the maximal slope of the spike-triggered average current (I_{STA}) (Fig. 9*C*) and reduced coherence with high-frequency input (Fig. 9*D*). Although the shape of the coherence-frequency relationship was somewhat different from that of PNs, the difference in coherence between the dynamic- and fixed-threshold models showed a peak at ~200 Hz (Fig. 9*E*), which was similar to the data from PNs (Fig. 7*C*).

How can a dynamic threshold increase coherence at high frequencies? Because of the threshold dynamics, $\theta(t)$ is low-pass filtered with respect to $V(t)$. Therefore, the threshold dynamics reduce the ability of low-frequency input to change the 'distance to threshold', $\theta - V$. When the input to a neurone is a mixture of many frequency components, each input frequency affects the timing of each spike. The dynamic threshold does not affect high-frequency signals directly, but reduces the influence of lower-frequency signals, allowing the high-frequency input to control spike timing. We demonstrated this by high-pass filtering the noise stimulus applied to the model (200 Hz cutoff frequency). In the absence of lower-frequency input, the dynamic threshold had much less effect on the high-frequency coherence (Fig. 9*F*). These simulations suggest that the dynamic spike threshold of PNs increases spike coherence with

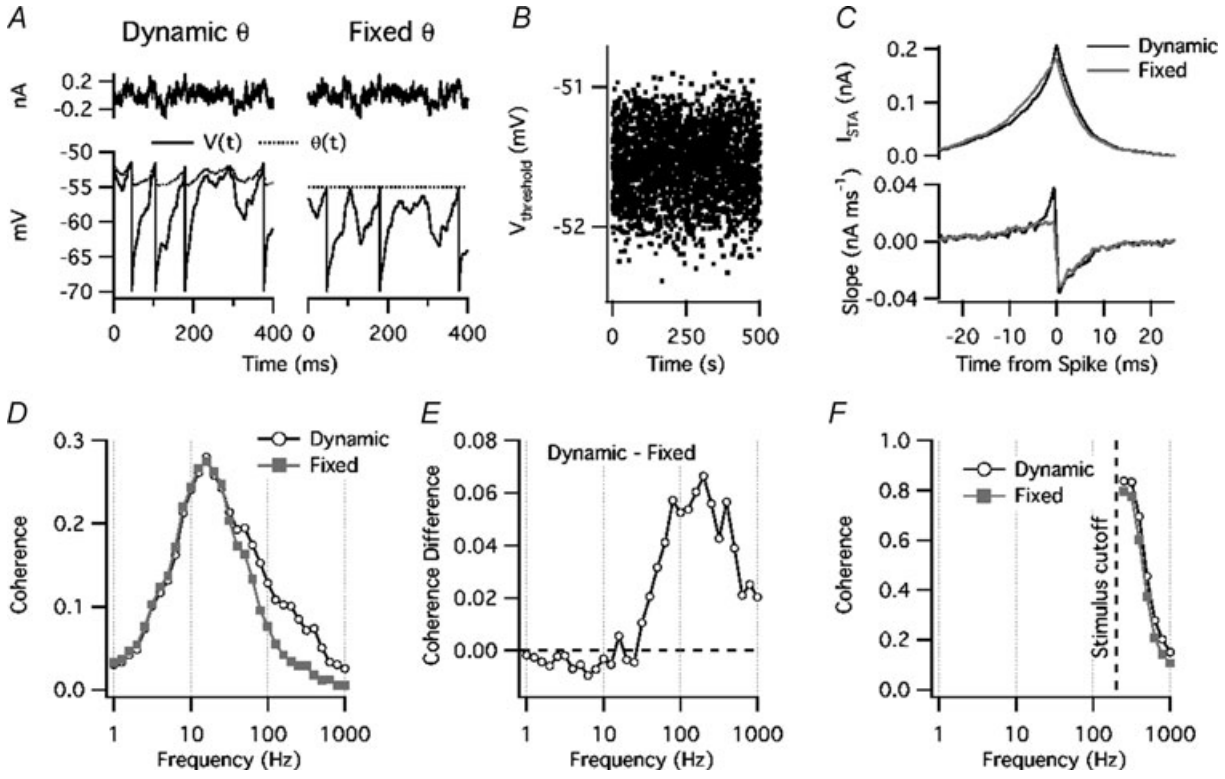

Figure 9. Dynamic threshold model: response to noise
A, top, noise current stimulus. Bottom, voltage response (continuous line) and threshold, $\theta(t)$ (dotted line). Each spike time can be identified by a voltage reset. Left, model with dynamic threshold. Right, model with fixed threshold. *B*, variation of threshold crossing voltage ($V_{\text{threshold}}$) for model with dynamic threshold. *C*, top, spike-triggered average current (I_{STA}) with dynamic threshold (black line) or fixed threshold (grey line). Bottom, slope of I_{STA}, taken over a 1 ms sliding window. *D*, coherence *versus* frequency for standard noise stimulus. Open symbols: model with dynamic threshold. Filled grey symbols: fixed threshold. *E*, difference in coherence between dynamic-threshold model and fixed-threshold model. *F*, coherence *versus* frequency for high-pass filtered noise stimulus (cutoff = 200 Hz).

high-frequency input by attenuating lower-frequency signals that affect spike timing. Interestingly, the dynamic threshold had little effect on the coherence with low-frequency input, either in PNs or in the model. This may reflect the nearly proportional effect of the dynamic threshold on all of the low-frequency signal components, combined with the small amplitude of voltage fluctuations driven by high-frequency input; however, a complete analysis of the factors that affect the coherence spectrum is beyond the scope of the present study.

Discussion

Channels contributing to threshold changes

Ever since the mechanisms of the action potential were elucidated, it has been known that Na^+ channel inactivation and K^+ channel activation can raise the spike threshold (Hodgkin & Huxley, 1952). However, the relative roles and interaction of these processes in various neurones are still not well understood. Our data suggest that Kv1 channels have a large effect on threshold dynamics in layer 2–3 PNs. Blocking Kv1 with DTX or 4-AP reduced threshold accommodation during EPSPs and current steps, reduced threshold variation during noise stimulation, and lessened the dependence of threshold on dI/dt. During noise stimulation, blocking Kv1 reduced the SD of $V_{threshold}$ by an average of 45%, corresponding to a 68% decrease in variance. These data may underestimate the true effect, because the threshold SD measured during Kv1 blockade was only slightly greater than the baseline voltage noise, and in some cases the remaining threshold variation showed little correlation with the stimulus (Fig. 5*B*).

A number of previous studies have suggested that sodium channel inactivation is partially responsible for threshold accommodation, based largely on measurements of the action potential rate of rise ('ROR'). Although the ROR depends on the balance of inward Na^+ current and outward K^+ current during the action potential upstroke, it is generally assumed that the Na^+ conductance active during the spike is much larger than the subthreshold conductances and activates much faster than the other spike-dependent conductances; under these conditions the Na^+ conductance will have a dominant effect on the maximal ROR. In cortical neurones, Azouz & Gray (2000) reported that the ROR was inversely correlated with the spike threshold during visual stimulation. In hippocampal neurones, Henze & Buzsáki (2001) found that the threshold and the ROR varied as a function of the preceding inter-spike interval, consistent with sodium inactivation contributing to threshold elevation caused by spikes. A recent modelling study (Platkiewicz & Brette, 2011) demonstrated that sodium inactivation will cause strong threshold accommodation in response to subthreshold voltage changes if the half-inactivation voltage is below the minimum threshold (determined by the sodium and leak conductances) and the voltage dependence of inactivation approaches the sharpness of activation. By effectively increasing the leak of the spike generator and raising the minimum threshold, activation of the Kv1 conductance might further increase threshold via sodium inactivation.

Despite these previous reports and modelling predictions, our data obtained using synaptic stimuli provided little evidence for sodium inactivation, showing only a very slight decrease in action potential rate of rise as a function of the EPSP-spike latency. However, these data do not directly indicate whether the axonal sodium channels responsible for spike initiation were inactivated, because the sodium channels responsible for spike back-propagation to the soma may have different properties (Hu *et al.* 2009) and experience a different voltage trajectory. This issue can only be resolved by different experimental techniques (e.g. voltage and sodium imaging of the spike initiation zone) and/or studies using selective toxins to alter fast sodium channel inactivation.

In addition to investigating the role of sodium inactivation, future studies will need to determine how the intricate spatial arrangement of channels in the AIS and nodes affects the spike threshold and its dynamics. Recent reports have shown that the distribution of sodium channels and their cytoskeletal attachments in the AIS shows activity-dependent plasticity (Grubb & Burrone, 2010; Kuba *et al.* 2010). To our knowledge, the corresponding changes in Kv1 channel localization have not been reported. However, changes in both sodium and potassium channel distributions might affect the threshold level and dynamics, and might thereby alter neuronal excitability, stimulus selectivity, and frequency response properties.

The high-pass function of threshold accommodation

Our data complement previous studies showing that threshold accommodation functions as a high-pass filter, enhancing the ability of neurones to encode fast signals. Azouz & Gray (2000) showed that a dynamic threshold could help neurones encode synchronous synaptic input, and Wilent & Contreras (2005) found that threshold changes increase the difference in output spike number between 'preferred' and 'non-preferred' inputs that depolarize cortical neurones at different rates. These findings may be explained by the analysis of Platkiewicz & Brette (2011), who demonstrated that the 'effective PSP' – the difference between the postsynaptic potential and the dynamic threshold – is smaller and briefer than the PSP itself. The amplitude of the effective PSP becomes

smaller when the PSP is broader. Thus, broad, slow-rising PSPs resulting from summation of asynchronous synaptic inputs are less able to elicit spikes than narrow, fast-rising PSPs caused by synchronous inputs.

Threshold accommodation caused by Kv1 may have similar functions in other types of neurones. The firing of fast-spiking (FS) cortical interneurones is strongly influenced by axonal Kv1 channels, which can delay the onset of firing and raise the threshold for the first spike (Goldberg *et al.* 2008). We would predict that the threshold increase and the delay can be overcome by sufficiently large, synchronous synaptic input, and thus Kv1 channels will favour coincidence detection by FS cells. Outside the cortex, auditory brainstem neurones show threshold accommodation that may contribute to their precise spike timing (Monsivais & Rubel, 2001; Howard & Rubel, 2010). While the ionic mechanisms of the threshold changes were not determined, these cells express high levels of Kv1 channels, which are known to enhance their spike timing precision in response to high-frequency synaptic input (Reyes *et al.* 1994; Koyano *et al.* 1996; Gittelman & Tempel, 2006).

Implications for spike timing

While Kv1 channels are commonly thought to 'improve spike timing', this may not be true under all conditions. When the signal is fast and the noise is relatively slow, Kv1 can reduce spike-timing jitter with respect to the signal (Fig. 6*D*). However, if the signal is slow and the noise is fast, Kv1 may increase jitter. A recent study reported that Kv1 increases spike timing jitter in hippocampal CA3 PNs stimulated with current steps or EPSC-like currents (Cudmore *et al.* 2010), experiments in which noise presumably arises from intrinsic channel fluctuations. The report did not indicate whether threshold dynamics contributed to the effects on jitter, which were explained at least in part by a change in dV/dt before each spike. Our experiments did not provide an ideal assay of jitter, because adjusting current steps to achieve a spike probability of ∼50% essentially showed half of the spike time distribution and may have introduced jitter due to the continuous adjustments. However, we observed a tendency toward lower jitter during Kv1 blockade for steps of 6 ms or longer ($P = 0.04$ for 6 ms, $P = 0.01$ for 12 ms, $P = 0.26$ for 24 ms), which may be apparent from the spike traces in Fig. 2*A* and *B*.

Rather than increasing precision for all signals, our data show that Kv1 channels cause spike timing to be influenced strongly by high-frequency components of the signal and/or the noise. A previous study quantified the sensitivity of PN spike timing (or time-varying spike probability) to high-frequency input by measuring the gain in response to multiple frequency components of a noise stimulus (Higgs & Spain, 2009). The gain is a measure of a neurone's input integration that is related to the coherence (varying with $c^{1/2}$) but also depends on the power spectrum of the stimulus and the output firing rate of the neurone. In PNs superfused with control ACSF and firing at 5–10 Hz, the gain was shown to peak at ∼400 Hz. Analysis of our present data showed that DTX or 4-AP greatly reduced this apparent 'high-frequency resonance' (Supplemental Figure).

Possible roles of Kv1-dependent accommodation in cortical oscillations and epilepsy

Based on our coherence analysis, the high-pass cutoff frequency imposed by Kv1 in L2–3 PNs is quite high (> 60 Hz). Thus, we do not expect Kv1 to improve spike timing with respect to low-gamma or slower oscillations. However, our results suggest that Kv1 may play a role in 'fast ripple' oscillations (> 200 Hz) that occur in epilepsy (Bragin *et al.* 1999*a*,*b*). These very fast oscillations in network activity and extracellular potential can arise from in-phase neuronal bursting or out-of-phase activity in groups of neurones, each firing action potentials at a rate lower than the peak frequency (Dzhala & Staley, 2004; Foffani *et al.* 2007; Ibarz *et al.* 2010; Köhling & Staley, 2011). While the net effect of Kv1 is clearly anticonvulsant, based on the strong convulsant activity of blockers including DTX, Kv1 channels might promote neuronal synchrony during fast ripple activity. Consistent with this idea, blocking potassium channels increased spike timing jitter in hippocampal PNs firing bursts of action potentials, and reduced the amplitude of fast ripples in the extracellular field potential (Dzhala & Staley, 2004). It would be of interest to investigate the specific roles of Kv1 channels in these effects.

References

Ashida G, Abe K, Funabiki K & Konishi M (2007). Passive soma facilitates submillisecond coincidence detection in the owl's auditory system. *J Neurophysiol* **97**, 2267–2282.

Azouz R & Gray CM (2000). Dynamic spike threshold reveals a mechanism for synaptic coincidence detection in cortical neurons in vivo. *Proc Natl Acad Sci U S A* **97**, 8110–8115.

Azouz R & Gray CM (2003). Adaptive coincidence detection and dynamic gain control in visual cortical neurons in vivo. *Neuron* **37**, 513–523.

Bekkers JM & Delaney AJ (2001). Modulation of excitability by α-dendrotoxin-sensitive potassium channels in neocortical pyramidal neurons. *J Neurosci* **21**, 6553–6560.

Benda J, Longtin A & Maler L (2005). Spike-frequency adaptation separates transient communication signals from background oscillations. *J Neurosci* **25**, 2312–2321.

Bragin A, Engel J Jr, Wilson CL, Fried I & Buzsáki G (1999*a*). High-frequency oscillations in human brain. *Hippocampus* **9**, 137–142.

Bragin A, Engel J Jr, Wilson CL, Fried I & Mathern GW (1999*b*). Hippocampal and entorhinal cortex high-frequency oscillations (100–500 Hz) in human epileptic brain and in kainic acid-treated rats with chronic seizures. *Epilepsia* **40**, 127–137.

Castle NA, Fadous S, Logothetis DE & Wang GK (1994). Aminopyridine block of Kv1.1 potassium channels expressed in mammalian cells and *Xenopus* oocytes. *Mol Pharmacol* **45**, 1242–1252.

Cudmore RH, Fronzaroli-Molinieres L, Giraud P & Debanne D (2010). Spike-time precision and network synchrony are controlled by the homeostatic regulation of the D-type potassium current. *J Neurosci* **30**, 12885–12895.

Dodson PD, Billups B, Rusznák Z, Szûcs G, Barker MC & Forsythe ID (2003). Presynaptic rat Kv1.2 channels suppress synaptic terminal hyperexcitability following action potential invasion. *J Physiol* **550**, 27–33.

Drummond GB (2009). Reporting ethical matters in *The Journal of Physiology*: standards and advice. *J Physiol* **587**, 713–719.

Du J, Zhang L, Weiser M, Rudy B & McBain CJ (1996). Developmental expression and functional characterization of the potassium-channel subunit Kv3.1b in parvalbumin-containing interneurons of the rat hippocampus. *J Neurosci* **16**, 506–518.

Dzhala VI & Staley KJ (2004). Mechanisms of fast ripples in the hippocampus. *J Neurosci* **24**, 8896–8906.

Farries MA, Kita H & Wilson CJ (2010). Dynamic spike threshold and zero membrane slope conductance shape the response of subthalamic neurons to cortical input. *J Neurosci* **30**, 13180–13191.

Foffani G, Uzcategui YG, Gal B & Menendez de la Prida L (2007). Reduced spike-timing reliability correlates with the emergence of fast ripples in the rat epileptic hippocampus. *Neuron* **55**, 930–941.

Gittelman JX & Tempel BL (2006). Kv1.1-containing channels are critical for temporal precision during spike initiation. *J Neurophysiol* **96**, 1203–1214.

Goldberg EM, Clark BD, Zagha E, Nahmani M, Erisir A & Rudy B (2008). K^+ channels at the axon initial segment dampen near-threshold excitability of neocortical fast-spiking GABAergic interneurons. *Neuron* **58**, 387–400.

Grasse DW & Moxon KA (2010). Correcting the bias of spike field coherence estimators due to a finite number of spikes. *J Neurophysiol* **104**, 548–558.

Grubb MS & Burrone J (2010). Activity-dependent relocation of the axon initial segment fine-tunes neuronal excitability. *Nature* **465**, 1070–1074.

Guan D, Lee JC, Higgs MH, Spain WJ & Foehring RC (2007). Functional roles of Kv1 channels in neocortical pyramidal neurons. *J Neurophysiol* **97**, 1931–1940.

Guan D, Lee JC, Tkatch T, Surmeier DJ, Armstrong WE & Foehring RC (2006). Expression and biophysical properties of Kv1 channels in supragranular neocortical pyramidal neurones. *J Physiol* **571**, 371–389.

Harvey AL & Robertson B (2004). Dendrotoxins: structure-activity relationships and effects on potassium ion channels. *Curr Med Chem* **11**, 3065–3072.

Henze DA & Buzsáki G (2001). Action potential threshold of hippocampal pyramidal cells in vivo is increased by recent spiking activity. *Neuroscience* **105**, 121–130.

Higgs MH, Slee SJ & Spain WJ (2006). Diversity of gain modulation by noise in neocortical neurons: regulation by the slow afterhyperpolarization conductance. *J Neurosci* **26**, 8787–8799.

Higgs MH & Spain WJ (2009). Conditional bursting enhances resonant firing in neocortical layer 2–3 pyramidal neurons. *J Neurosci* **29**, 1285–1299.

Hill AV (1936). Excitation and accommodation in nerve. *Proc R Soc B* **119**, 305–355.

Hodgkin AL & Huxley AF (1952). A quantitative description of membrane current and its application to conduction and excitation in nerve. *J Physiol* **117**, 500–544.

Howard MA & Rubel EW (2010). Dynamic spike thresholds during synaptic integration preserve and enhance temporal response properties in the avian cochlear nucleus. *J Neurosci* **30**, 12063–12074.

Hsiao CF, Kaur G, Vong A, Bawa H & Chandler SH (2009). Participation of Kv1 channels in control of membrane excitability and burst generation in mesencephalic V neurons. *J Neurophysiol* **101**, 1407–1418.

Hu W, Tian C, Li T, Yang M, Hou H & Shu Y (2009). Distinct contributions of $Na_v1.6$ and $Na_v1.2$ in action potential initiation and backpropagation. *Nat Neurosci* **12**, 996–1002.

Hutcheon B & Yarom Y (2000). Resonance, oscillation and the intrinsic frequency preferences of neurons. *Trends Neurosci* **23**, 216–222.

Ibarz JM, Foffani G, Cid E, Inostroza M & Menendez de la Prida L (2010). Emergent dynamics of fast ripples in the epileptic hippocampus. *J Neurosci* **30**, 16249–16261.

Inda MC, DeFelipe J & Muñoz A (2006). Voltage-gated ion channels in the axon initial segment of human cortical pyramidal cells and their relationship with chandelier cells. *Proc Natl Acad Sci U S A* **103**, 2920–2925.

Köhling R & Staley K (2011). Network mechanisms for fast ripple activity in epileptic tissue. *Epilepsy Res* (in press).

Kole MH, Letzkus JJ & Stuart GJ (2007). Axon initial segment Kv1 channels control axonal action potential waveform and synaptic efficacy. *Neuron* **55**, 633–647.

Kole MH & Stuart GJ (2008). Is action potential threshold lowest in the axon? *Nat Neurosci* **11**, 1253–1255.

Koyano K, Funabiki K & Ohmori H (1996). Voltage-gated ionic currents and their roles in timing coding in auditory neurons of the nucleus magnocellularis of the chick. *Neurosci Res* **26**, 29–45.

Kuba H, Ishii TM & Ohmori H (2006). Axonal site of spike initiation enhances auditory coincidence detection. *Nature* **444**, 1069–1072.

Kuba H, Oichi Y & Ohmori H (2010). Presynaptic activity regulates Na^+ channel distribution at the axon initial segment. *Nature* **465**, 1075–1078.

LeFevre (1950). Excitation characteristics of the squid giant axon: a test of excitation theory in a case of rapid accommodation. *J Gen Physiol* **34**, 19–36.

Lorincz A & Nusser Z (2008). Cell-type-dependent molecular composition of the axon initial segment. *J Neurosci* **28**, 14329–14340.

Massengill JL, Smith MA, Son DI & O'Dowd DK (1997). Differential expression of K4-AP currents and Kv3.1 potassium channel transcripts in cortical neurons that develop distinct firing phenotypes. *J Neurosci* **17**, 3136–3147.

Monsivais P & Rubel EW (2001). Accommodation enhances depolarizing inhibition in central neurons. *J Neurosci* **21**, 7823–7830.

Naundorf B, Wolf F & Volgushev M (2006). Unique features of action potential initiation in cortical neurons. *Nature* **440**, 1060–1063.

Ogawa Y, Horresh I, Trimmer JS, Bredt DS, Peles E & Rasband MN (2008). Postsynaptic density-93 clusters Kv1 channels at axon initial segments independently of Caspr2. *J Neurosci* **28**, 5731–5739.

Palmer LM & Stuart GJ (2006). Site of action potential initiation in layer 5 pyramidal neurons. *J Neurosci* **26**, 1854–1863.

Platkiewicz J & Brette R (2011). Impact of fast sodium channel inactivation on spike threshold dynamics and synaptic integration. *PLoS Comput Biol* **7**, e1001129.

Reyes AD, Rubel EW & Spain WJ (1994). Membrane properties underlying the firing of neurons in the avian cochlear nucleus. *J Neurosci* **14**, 5352–5364.

Rothman JS & Manis PB (2003). Kinetic analyses of three distinct potassium conductances in ventral cochlear nucleus neurons. *J Neurophysiol* **89**, 3083–3096.

Russell SN, Publicover NG, Hart PJ, Carl A, Hume JR, Sanders KM & Horowitz B (1994). Block by 4-aminopyridine of a Kv1.2 delayed rectifier K^+ current expressed in *Xenopus* oocytes. *J Physiol* **481**, 571–584.

Shu Y, Yu Y, Yang J & McCormick DA (2007). Selective control of cortical axonal spikes by a slowly inactivating K^+ current. *Proc Natl Acad Sci U S A* **104**, 11453–11458.

Slee SJ, Higgs MH, Fairhall AL & Spain WJ (2005). Two-dimensional time coding in the auditory brainstem. *J Neurosci* **25**, 9978–9988.

Stafstrom CE, Schwindt PC & Crill WE (1984). Repetitive firing in layer V neurons from cat neocortex in vitro. *J Neurophysiol* **52**, 264–277.

Stephens GJ, Garratt JC Robertson B & Owen DG (1994). On the mechanism of 4-aminopyridine action on the cloned mouse brain potassium channel mKv1.1. *J Physiol* **477**, 187–196.

Stuart G, Schiller J & Sakmann B (1997). Action potential initiation and propagation in rat neocortical pyramidal neurons. *J Physiol* **505**, 617–632.

Svirskis G, Kotak V, Sanes DH & Rinzel J (2002). Enhancement of signal-to-noise ratio and phase locking for small inputs by a low-threshold outward current in auditory neurons. *J Neurosci* **22**, 11019–11025.

Uhlenbeck GE & Ornstein LS (1930). On the theory of brownian motion. *Phys Rev* **36**, 823–841.

Wilent WB & Contreras D (2005). Stimulus-dependent changes in spike threshold enhance feature selectivity in rat barrel cortex neurons. *J Neurosci* **25**, 2983–2991.

Yu Y, Shu Y & McCormick DA (2008). Cortical action potential backpropagation explains spike threshold variability and rapid-onset kinetics. *J Neurosci* **28**, 7260–7272.

Zhou L, Messing A & Chiu SY (1999). Determinants of excitability at transition zones in Kv1.1-deficient myelinated nerves. *J Neurosci* **19**, 5768–5781.

Author contributions

The experiments were performed in the laboratory of W.J.S., who contributed to the conception and design of the experiments, the interpretation of data, and critical revision of the article. M.H.H. contributed to the conception and design of the experiments, collected and analysed the data, and drafted and revised the article.

Acknowledgements

This material is based on work supported by the US Department of Veterans Affairs, Office of Research and Development, Biomedical Laboratory Research Program. Funding was provided by a Veterans Affairs Merit Review to W.J.S. and a Veterans Affairs Epilepsy Centre of Excellence. We thank Robert Foehring and Adrienne Fairhall for helpful discussions, Steve Redman for helpful comments on the manuscript, and Susan Usher for excellent technical assistance.